Article:
Zhou, L., Brunskill, H. and Lewis, R. orcid.org/0000-0002-4300-0540 (2022) Experimental investigation on ball plate contact using ultrasonic reflectometry : from static to dynamic. Ultrasonics, 124. 106733. ISSN 0041-624X

https://doi.org/10.1016/j.ultras.2022.106733

Experimental Investigation on Ball Plate Contact Using Ultrasonic Reflectometry: From Static to Dynamic

Lu Zhou[1, 2, *], Henry Brunskill[1], Roger Lewis[1]

[1] Leonardo Centre, Department of Mechanical Engineering, The University of Sheffield, Mappin Street, S1 3JD, Sheffield, United Kingdom

[2] Department of Civil and Environmental Engineering, The Hong Kong Polytechnic University, Hung Hom, Kowloon, Hong Kong S.A.R.

[*] Correspondence: zhoul540@gmail.com, lu.lz.zhou@polyu.edu.hk

Abstract

Machine elements such as rolling element bearings are widely used in engineering and transportation areas. The life of a bearing is closely related to the stress state in the constituent components. Determining the stress state experimentally is difficult since the contact region is hidden inside the contacting bodies, making it difficult to characterize without altering the contact itself. This paper presents an experimental study to monitor static and dynamic ball-on-flat contacts, by using an ultrasonic reflectometry measuring technique, to demonstrate the concept of monitoring operating ball-bearing conditions in a non-invasive manner. By using an ultrasonic focusing probe and a 64-element ultrasonic array, contacts between a nitrile ball and a Perspex plate as well as contact between a steel ball and a grooved steel plate were characterised under both static and dynamic conditions. Both contact size and distribution of contact stress can be visualized in 2-dimensional plots. In this paper, the capability of ultrasonic reflectometry for non-invasive characterisation of contact conditions are demonstrated, and more importantly the development of multiple measuring mechanisms to realize real-time contact monitoring from static to dynamic conditions is illustrated. The proposed technique in the study is expected to characterise dynamic contacts of bearings in various scenarios from small mechanical systems (e.g., micro motors) to large civil infrastructures (e.g., wind turbines).

Keywords: Structural health monitoring, Ultrasonic testing, Contact mechanics, Ultrasonic array, Non-destructive evaluation

1. Introduction

The wear and deterioration problem of rolling element bearings has concerned researchers and operators for many years. There have been numerous studies on the wear evolution of rolling element bearings including theoretical analysis [1-3], numerical simulations [4, 5], and experimental investigations [6-9], etc. Many studies focus on the macro-scale manifestation of wear behaviour to understand the evolving mechanisms, while under certain circumstances it is more important to research into the

root cause of wear and failures. For bearings and railway systems, the interfacial contact conditions between roller and raceways or wheel and rail are dominant factors in driving wear, plastic flow and cracks in the interacting surfaces. Therefore, characterisation of machine element contacts is essential in these situations. Over the past century since Hertz theory was first established in 1882 [10], increasingly refined and sophisticated analytical and numerical models have been proposed based on theories from classical half-space assumptions [11,12] to fractal modelling of surface roughness distributions [13-15]. Each of these models predicts contact conditions with satisfactory performance corresponding to specific circumstances and can be used as good verification methods. However, due to the complexity of contacting profiles and the stochasticity of surface roughness, both theoretical predictions and finite-element simulations cannot fully reveal the conditions in realistic contacts. Yet for in-service machine elements, optimum contact conditions are paramount to safety and reliability. In terms of bearings and wheel-rail systems, such demands are further elevated to real-time monitoring of dynamic contacts in operation. Different techniques have been developed in previous work, attempting to capture the transient contact characteristics including air flows [16], electrical resistance [17], photoelasticity [18], and pressure films [19, 20]. Nevertheless, the contact information acquired from these techniques is rather limited and, in most cases, can only provide an estimation of the contact area. More importantly, despite some being classified as "non-destructive" tests, all of the above measuring techniques intrude in the contact region and inevitably alter the characteristics of contact. Since the contact zones are the connecting regions between two contacting bodies and are hard to reach, it is tricky for conventional techniques to characterise the conditions without intrusion. For contact condition monitoring, it is desirable to seek approaches that are not only non-destructive, but also non-invasive. There are also some other options to monitor the contact patch by using thermal imaging [21] or computer vision [22], but neither thermal device nor cameras can penetrate into the actual contact regions. In summary, when it comes to real-time dynamic contact characterisation, existing monitoring techniques are hindered by the trade-off between access to contact regions and non-invasive design, making the task challenging.

Ultrasonic measuring techniques have been widely applied in many disciplines including engineering and medical sectors with mature commercialisation. In particular, ultrasonic reflectometry has been proved as an effective technique in contact characterisation. This technique eliminates the trade-off problem by emitting ultrasonic beams that precisely strike at the contacting interfaces without any influence on the contact patch. Previous work has demonstrated the use of ultrasonic reflectometry in characterising static contacts between different machine elements including wheel-rail specimens [23], bolted joints [24] and sealing tubes [25] with 2-dimensional (2D) plots showing contact stress distribution. Apart from static cases, measurement of oil film thickness has also been investigated using ultrasound for contacts in the elastohydrodynamic lubrication (EHL) regime [26, 27], but the investigation only considered one-point measurement and cannot give a map of contact conditions. Previous research carried out by the authors presents a pilot study on characterization

of wheel-rail contacts which are metal-metal contacts, while in this study we attempt to look into small rolling contacts and non-metal contacts with nonlinear behaviour [28, 29, 30].

For easy demonstration purposes, static and dynamic contacts between a nitrile ball and a Perspex plate were investigated first. Rolling and sliding cases were investigated respectively for nitrile ball-Perspex plate contact. The transparency of Perspex provides an additional way to validate the ultrasonic measurements with images alongside Hertz predictions. Subsequently, the experimental study was extended to static and dynamic contacts between a steel ball and a grooved plate that mimics the contacts of a roller bearing. To the author's knowledge, it is for the first time that non-metal contacts with large deformation and nonlinear behaviours are investigated through ultrasonic reflectometry, which is expected to satisfy a greater range of applications.

2. Principle of ultrasonic reflectometry

Ultrasound refers to sound waves with a propagating frequency higher than the upper audible threshold of human hearing (normally 20kHz). According to the propagating behaviour of ultrasound, ultrasonic measuring techniques can be roughly classified into two main categories: surface wave-based techniques and body wave-based techniques. Representative surface wave-based techniques such as ultrasonic guided wave (UGW) testing have been widely used in industrial and transportation areas and are particularly effective for flaw detection of thin-wall structures [31-33]. On the other hand, ultrasonic reflectometry is a typical body wave-based technique that reveals health conditions of structures or human tissues based on information of reflected sound waves and has been extensively applied in medical diagnosis and inspection of industrial components from a cross-sectional perspective [34, 35]. The application of ultrasonic reflectometry in contact characterisation focuses on the interactions between ultrasonic compression waves (p-wave) and contacting interfaces at a relatively micro-scale (micrometre scale). When it comes to a machine element, no matter how well the surface is finished, at the micro-scale the surface has roughness, which is manifested as a random distribution of asperities, as shown in Figure 1(a). When the surfaces of two bodies are pressed together under compressive load, it is these asperities that come into contact, leaving air gaps in between. As illustrated in Figure 1(b), the asperities at the interface can be modelled as a series of springs with a total stiffness K, which is defined as the first-order derivative of the nominal contact pressure p with respect to the mean separation u between two interfaces:

$$K = -\frac{dp}{du} \tag{1}$$

When a beam of ultrasonic waves strikes at the interface, it will be partially reflected and partially transmitted. Kendall and Tabor thoroughly investigated the interacting behaviours between ultrasonic waves and the springs [36] and found that when the wavelength of the ultrasonic wave is long compared to the length of air gaps, the interface acts as a single reflector, and the ultrasonic reflection is determined by the spring stiffness. The ratio of the reflected signal and incident signal, known as the

reflection coefficient, R , has a relationship with interfacial stiffness K as shown below:

$$R = \frac{z_2 - z_1 + i\ (z_1 z_2 / K)}{z_2 + z_1 + i\omega (z_1 z_2 / K)} \tag{2}$$

where $\omega = 2\pi f$ is the angular frequency of the ultrasonic waves, z_1 and z_2 is the acoustic impedance of the two contacting materials respectively and is determined as:

$$z = \rho c \tag{3}$$

where ρ is the density and c the speed of sound in the material. Because both density of air and the sound speed in air is significantly lower than the corresponding values of the machine element materials, most energy of the ultrasonic waves will be reflected at the air gaps. For two contacting bodies made of same or similar materials, most ultrasonic energy will be transmitted through the asperity contact area. As the normal compression load increases, the asperities deform, and more asperities come into contact leading to an increase in K and a decrease in R since more energy is transmitted. Considering a monitoring area divided into multiple sections, by either moving the ultrasonic transducer in a plane or implementing the monitoring area with array/matrix of sensors and measuring the waveforms of incident and reflected ultrasonic waves, the average value of the reflection coefficient of each section can be obtained, forming up a 2D map of R, and subsequently 2D distribution of K indicating the contact conditions.

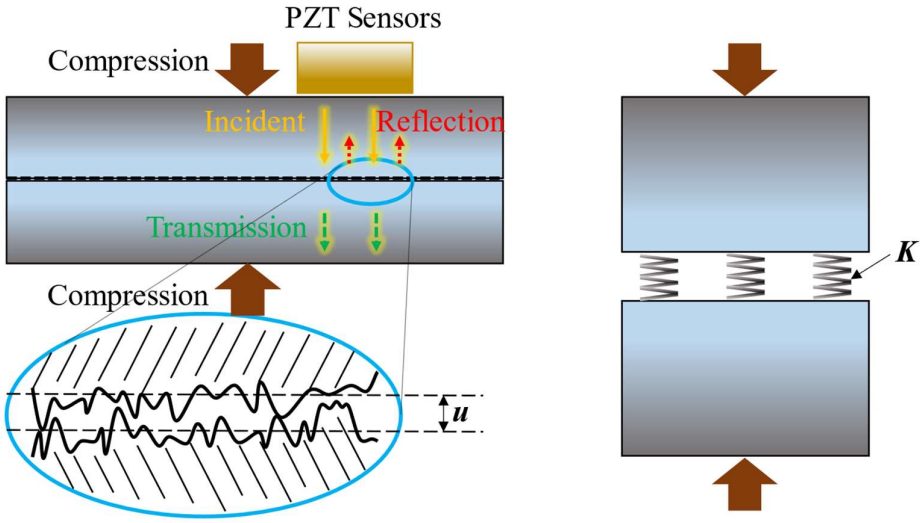

(a) (b)

Figure 1. (a) a diagram showing to scale the surface asperities coming into contact and (b) how the interface behaves as a series of springs of stiffness ***K***.

Theoretically, the interfacial stiffness ***K*** increases non-linearly from zero when two surfaces are at the point of first contact under zero load, to infinity when there is no air gap between them. To further correlate ***K*** with contact pressure ***p***, Drinkwater et al. [37] found that, for a given roughness pair of two contacting surfaces, there is a unique

relationship between contact stiffness and contact pressure. In practice for most machine element contacts when the contact pressure is relatively low and does not exceed yield strength, the relationship is approximately linear. For each contact, a calibration test needs to be carried out over a known contact patch with the same surface roughness level as that of the test specimens, and the relationship between contact pressure and interfacial stiffness can be subsequently established. For the non-metal contact to be investigated in this study, linear relationship is no longer accurate, and a specific calibration test needs to be conducted.

3. Nitrile ball-Perspex plate contact characterisation

Contacts between a 13mm-radius nitrile ball and a Perspex plate were investigated first in this study, since the high flexibility of nitrile material enables a larger contact patch to form, which can demonstrate well the contact distributions in detail for both static and dynamic cases by using ultrasonic reflectometry. Using a nitrile ball can also guarantee the contact is within the elastic range, and the result can be easily compared with other methods. Besides, the transparency of Perspex provides an additional way to visually validate the contact size by taking pictures of the contact patch. Specific properties of the two materials used are listed in Table 1.

Table 1. Properties of Nitrile and Perspex

Material	Density (kg/m^3)	Speed of sound under 5MHz longitudinal wave (m/s)	Young's modulus (MPa)	Poisson's ratio	Acoustic impedance
Nitrile	1200	1600	4	0.48	1920000
Perspex	1160	2730	3200	0.37	3166800

The Young's moduli and Poisson's ratios of the nitrile ball and the Perspex plate were obtained from data sheet values of butadiene rubber [38] and polymethyl-methacrylate (PMMA) [39] respectively. The density of each was determined by the weight of the specimen and the volume difference as the specimen was immersed in the water. The speed of sound was determined from a time-of-flight measurement of an longitudinal ultrasonic pulse at 5MHz through a specimen. The acoustic impedance of nitrile is significantly smaller than that of Perspex, but as the density of $1.2kg/m^3$ and the speed of sound in air is around 340m/s, there is still a distinct difference between reflections from air gaps and those from asperity contacts, which enables the contact characterisation using the technique.

Measurement of static and dynamic contacts were taken using two test configurations described below.

3.1 Instrumentation and test set-up

3.1.1 Static Test

To characterise static contacts, an ultrasonic focusing probe was used for scanning. Figure 2 shows the inner structure of an ultrasonic probe. When the piezo-electric wafer is subject to high-frequency alternating voltage through the electrodes on two sides, it will oscillate correspondingly and generate ultrasonic pressure waves, which can only be emitted through the exist face, since emissions on all other directions are critically attenuated. When the piezo-electric wafer senses high-frequency vibrations, it will generate electric charges. In this way an ultrasonic probe can serve as both ultrasound pulser and receiver.

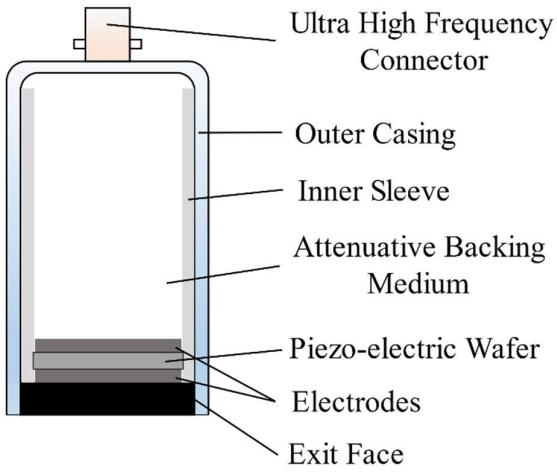

Figure 2. Inner structure of an ultrasonic focusing transducer.

Ultrasonic focusing probes come with a variety of centre frequencies (1MHz, 2MHz, 5MHz, 10MHz and 25MHz, etc.) and focal lengths. In principle, probes with higher centre frequency have higher energy and smaller focal spot size and thus can achieve higher resolutions in 2D scanning results [40] with diameter of the focal spot calculated as:

$$SpotDiameter\text{(-6dB)}=1.025\frac{l_w c_w}{f d_c} \tag{4}$$

where c_w and l_w is the speed of sound and the focal length of the transducer in water respectively, and d_c the diameter of the piezo-electric crystal. However, if the centre frequency is too high, it will suffer from severe attenuation and will penetrate less material within the specimen to be measured. In this study, a 5MHz probe was used as an optimized trade-off option between high quality scanning and acceptable signal attenuation. More comprehensive investigation on the frequency influence and optimum selection can be found in [41]. The focal spot diameter of a 5MHz probe is around 0.1mm and the scan was configured to 10mm*10mm area with 200 steps in the x and y directions. As a consequence, there were area overlaps between two neighbouring measurements in the static test, but this does not affect the integrity of the measurement.

It should be noted that although there are air-coupled ultrasonic transducers [42], they are basically applied for relatively low-frequency ultrasonic testing and cannot satisfy

the need for precise contact measurement in this study. As the frequency of the ultrasonic transducers used for contact characterisation should normally be higher than 1MHz to achieve a relatively high scanning resolution, a couplant is needed to avoid signal loss. In the static test, since the focal length of the transducer is relatively long, a water couplant with adequate depth (normally larger than 10mm) is needed to focus signals, while in the dynamic test, a water-based/oil-based couplant or glue is adequate for the ultrasonic array. It should be noted that longitudinal body waves are used for measurement and characterization, as shear waves cannot transmit through liquid.

A loading frame was built up for static measurements, as shown in Figure 3. A round Perspex plate was fixed on the top of the loading rig. A nitrile ball was placed in a ball holder to keep it still during the test. The load was applied through three compression springs which had been pre-calibrated to obtain the stiffness. By compressing the springs through the loading jack at the bottom of the loading frame for a known distance, the load can be applied correspondingly. The ultrasonic probe was immersed in the water couplant to focus the ultrasonic signals. The height of the ultrasonic probe can be adjusted so that the maximum energy of ultrasonic beam is focused precisely at the contact interface, hence the second reflection is more distinguishable and can be more easily extracted.

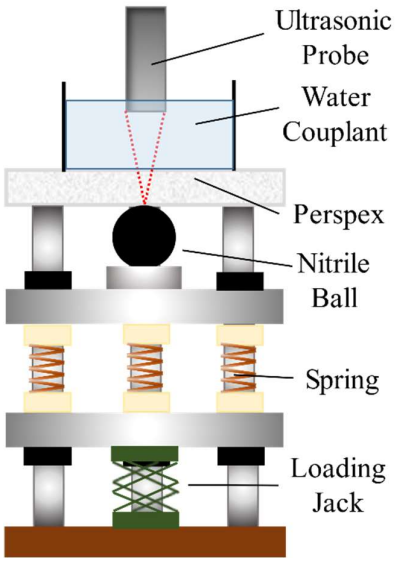

Figure 3. Static spring loading frame.

The loading frame was clamped on a large scanning tank, as shown in Figure 4. The scanning tank is able to move in a plane along x and y axis with two stepping motors. During the scanning process, the movable arm proceeds step-by-step along a winding line (see Figure 4). A series of measurements can be obtained from each individual scan. By reducing the step length, the resolution of the scan can be enhanced.

According to a Hertz prediction, the diameter of the contact patch between a 13mm diameter nitrile ball and a Perspex plate is smaller than 10mm, the scanning area was therefore set to be a 10mm*10mm square. The step-length along x and y directions were both set to be 0.1mm, and consequently each scan delivered a 100*100 matrix.

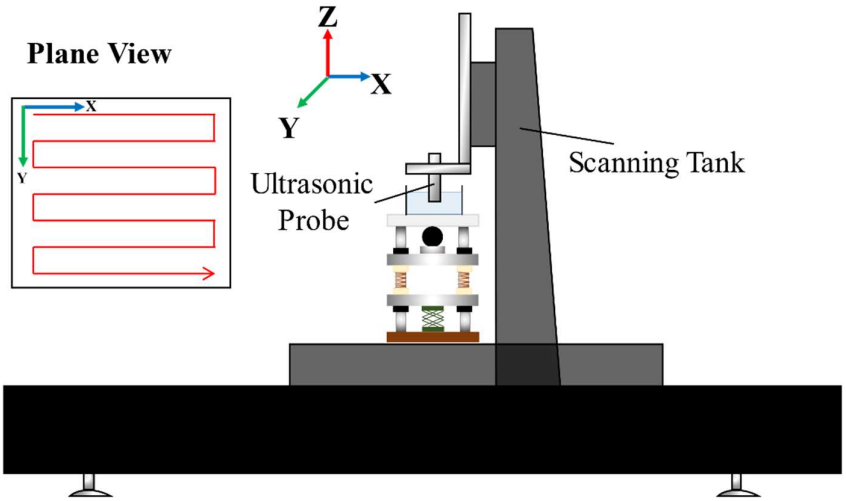

Figure 4. Scanning tank for static contact characterisation.

3.1.2 Dynamic Test

For dynamic contact characterisation, a 5MHz ultrasonic array was used. The array contains 64 sensing elements that are linearly placed in a 40mm long housing, as shown in Figure 5. A PC with an integrated National Instrument 8-channel data acquisition (DAQ) card was used to apply and receive voltages from the array. The entire system includes an ultrasonic pulser and receiver (FMS UPR, Tribosonics Ltd, UK) and a digitiser (FMS-100 Digitiser, Tribosonics Ltd, UK) with specifications shown in Table 2. Since the DAQ card can at most pulse and receive eight ultrasonic signals simultaneously, a multiplexer was used for switching between each 8-element subset. The switching speed can be so high (up to 10kHz) that when monitoring contacts with relatively low speed, it can be considered that all 64 elements pulse and receive at the same time. It is worth notifying that the FMS (or any decent ultrasonic pulser-receiver) is specifically designed to limit this type of signal distortion. The FMS has a signal bandwidth of 25MHz (the -6dB analogue bandwidth is 0.1 to 25MHz), so it will handle signals up to this frequency with little distortion or attenuation.

Table 1. Specifications of the DAQ system.

FMS UPR	
Switched input impedance	50/100/200/500R (50 ohm used)
Input attenuator	0/-20/-40 dB
Input preamp	+20dB
Receiver gain	+90dB
-6dB Bandwidth	0.1 to 25MHz
Bandpass filters	0.5/1/2.5/5/10/15MHz (10MHz used)
Dynamic range	>80dB
Channel crosstalk isolation	>80dB
Receiver noise	1.3nV/√Hz to 2nV//√Hz
Pulser output	-20V to-350V inverted “top-hat”
Rise and fall times	5ns ±1ns

Pulse width	10ns to 2μs in 10ns steps
Global PRF	100kHz max.
FMS-100 Digitiser	
Sampling frequency	100MHz
Resolution	12bit
Analogue bandwidth	25MHz
Noise	60dB SNR
Gates	6 real time in hardware
Software	Bespoke NI Labview code

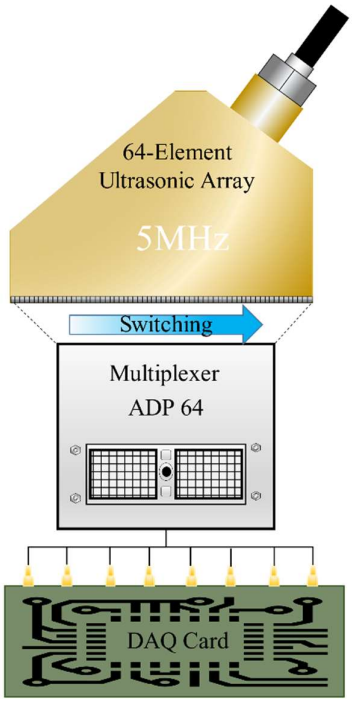

Figure 5. Channel switching of ultrasonic array

A mechanism was developed to carry out dynamic ball-on-flat tests, as shown in Figure 6. The nitrile ball which was used in static test was placed in between two Perspex plates to allow free rolling along one direction. The bottom Perspex plate was clamped on a moving base which was driven by a servo motor. The top Perspex plate was constrained to avoid lateral displacement and weights were symmetrically placed on the plate for even vertical loading. The 64-element ultrasonic array was fixed on top of the top plate to scan. As a test was in progress, the bottom plate moved forward and actuated the ball to roll. When the nitrile ball rolled over the scanning region, the contact between the nitrile ball and the top plate was captured and characterised. The water-based couplant adopted in the dynamic test has high viscosity, so that the thickness of the couplant does not vary in the rolling condition. For real application, semi-permanent glue can be used as the couplant to avoid the couplant deforming or moving.

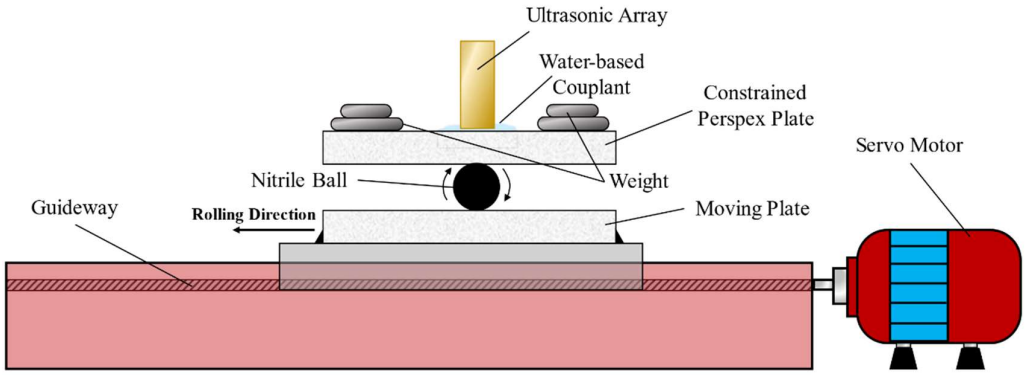

Figure 6. Set-up of the dynamic nitrile ball-Perspex plate contact test.

In the dynamic test, the speed was altered from 2mm/s to 10mm/s and 20mm/s by switching the motor speed, and 1kg to 5kg weights, at 1kg steps, were placed on the top plate to keep a consistency with the static loading. The bottom plate was pushed for a fixed length of 50mm each time. The ultrasonic array is 40mm long in the lateral direction, so each scan covers a 40mm*50mm rectangular region. Ultrasonic signals were emitted from 8 elements each time and reflected at the contact surface. As the switching speed of the pulsing channels is much faster than the rolling speed of the ball, it can be assumed that a line of 64 measurements were taken simultaneously. By merging the linear measurements from the whole rolling test, a 2D map of reflected voltage can be obtained. Subsequent procedures for data processing were the same as those in the static test. As the Perspex plate used in the dynamic test was made from same material with same surface finish (surface roughness), the calibration model in static test can also be transferred to the dynamic scenarios.

3.2 Results

Figure 7(a) displays the A-scan of a single measurement from the nitrile ball-Perspex plate contact test. Two reflections can be seen in one measurement. The first wave packet is the reflection from the top surface of the Perspex plate, and the second is the reflection from the contact interface. As ultrasonic signals are focused on the contact interface, the amplitude of the first reflection is much smaller than that of the second reflection. It is the second reflection that is of interest and peak-to-peak values were measured for this in each test. The peak-to-peak value is selected by firstly identifying the approximate position in the time scale of the reflection at the contact interface by measuring the total propagation distance (in both the water couplant and scanned object) with corresponding propagation speed. This position can be further confirmed through a preliminary test to check the wavelet package with varying amplitude with and without contact. Once the position along the time axis is identified, a window (comprised of two longitudinal cursors in the oscilloscope) is added to cover the reflection of interest, and the largest peak-to-peak value within the windowed region is extracted as one measurement.

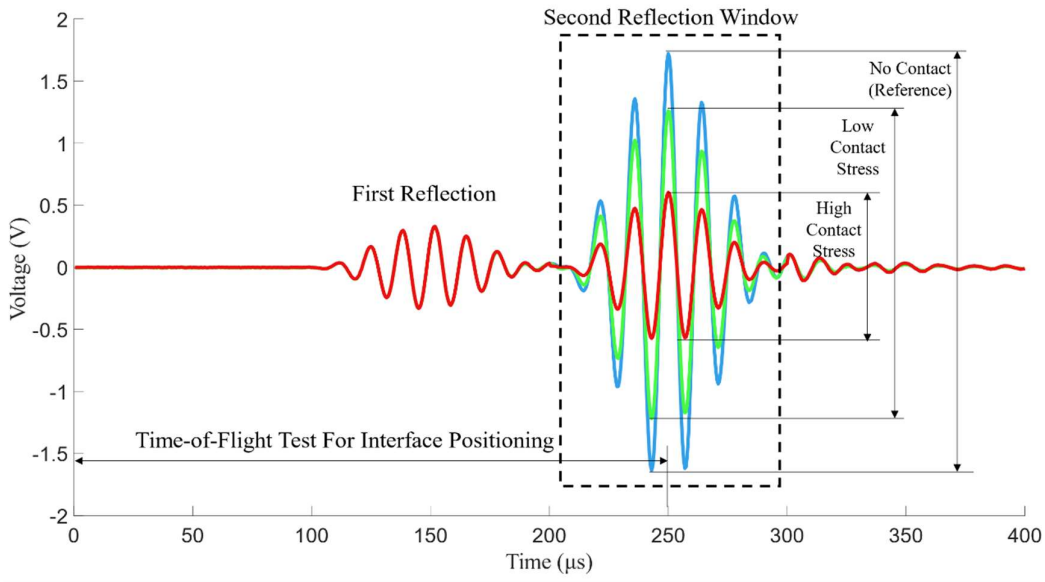

(a)

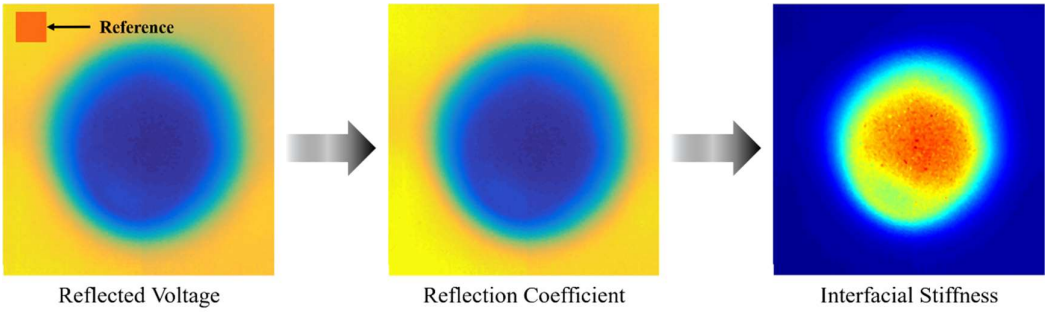

(b)

Figure 7. Data processing: a). peak-to-peak value extraction from A-scan measurement; b) from reflected voltage to contact stiffness.

As shown in Figure 7(b), the measured peak-to-peak values form a 2D matrix of reflected voltage. The reflection coefficient map was obtained by dividing the reflected voltage map by a reference measurement where no contact takes place to eliminate the influence of surface profile that is not perpendicular to the striking direction of the ultrasonic beam, as well as taking account of attenuation in the specimen material. Since the plate was assumed to be perfectly flat, a solitary reference value is enough for this case. The reference value was averaged from voltage measurements in the non-contact region. By taking modulus on both sides of Equation 2, the interfacial stiffness could be obtained as:

$$K = \omega z_1 z_2 \sqrt{\frac{1-|R|^2}{|R|^2(z_2+z_1)^2-(z_2-z_1)^2}} \tag{5}$$

From Equation 5 it can be seen that the reflection coefficient should be less than 1 and larger than $\frac{z_2-z_1}{z_2+z_1}$ to obtain positive stiffness that is meaningful, which can also be

referred from [23, 24]. For the nitrile ball-Perspex plate case, the reflection coefficient range was within $\frac{z_2-z_1}{z_2+z_1}$ to 1 referring to Table 1, and measurements higher than 1 or lower than $\frac{z_2-z_1}{z_2+z_1}$ due to perturbations (environmental noise, electrical interferences, and measuring error, etc.) were replaced with interpolations from neighbouring data. However, it should be noted that the theoretical smallest reflection coefficient value $\frac{z_2-z_1}{z_2+z_1}$ can only be achieved when in full contact, which is not possible in the real case, as the two contact surfaces cannot be fully pressed together with no air gap in between. Eventually, a map of interfacial stiffness could be plotted.

3.2.1 Calibration test

Since surface roughness dominates the relationship between interfacial stiffness $\boldsymbol{K}$ and contact pressure $\boldsymbol{p}$, a calibration was carried out by using the same loading frame and Perspex plate in contact with a 3mm radius, 1mm thick nitrile disc. The nitrile disc was cut from another nitrile ball which is identical to the specimen used in this study in terms of surface finish. The nominal radius of the contact patch was also 3mm so that the pressure range of interest could be fully covered. Loads from 10N to 60N, at 10N steps, were applied in the calibration test. Figure 8 shows the reflection coefficient and interfacial stiffness maps.

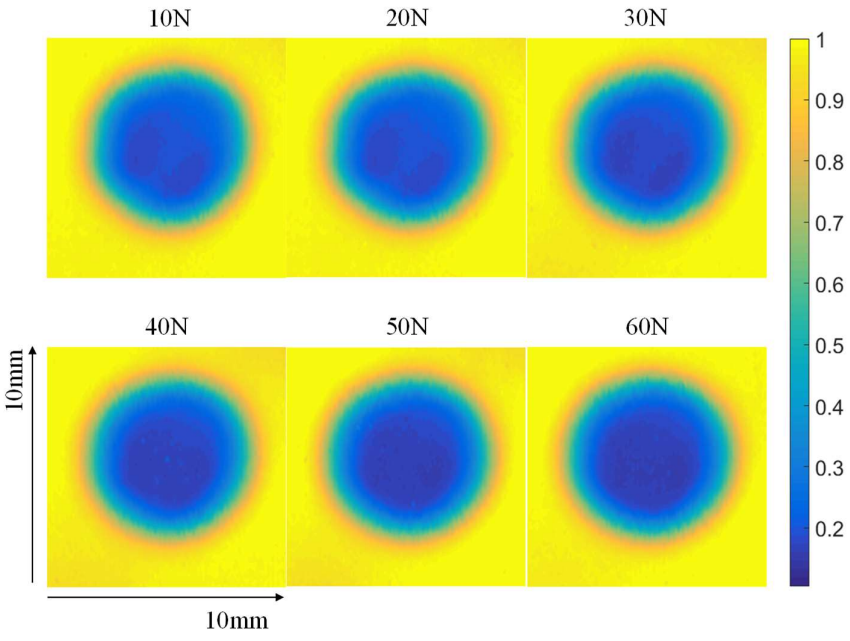

(a)

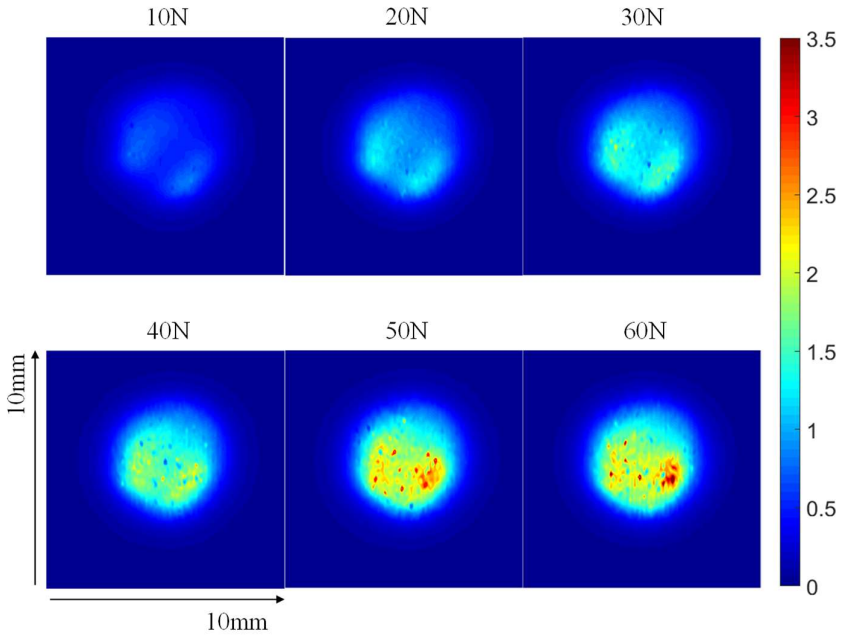

(b)

Figure 8. Distribution maps of: (a) reflection coefficient; (b) interfacial stiffness (GPa/μm) in calibration test.

One of the primary differences in dealing with non-metal contacts in this study in comparison to metal-metal contact characterisation is the large nonlinear deformation. As the authors' team have investigated previously, the ***K-p*** relationship for metal-metal contact with small deformation is normally close to linear relationship [41], and the contact pressure in a calibration test can be approximated as being evenly distributed, therefore the ***K-p*** relationship can be easily established through linear fitting. While for the non-metal contact in this study, firstly, the increment of ***K*** does not go up linearly with increasing normal load applied , the higher the normal load, the lower the interfacial stiffness increase. Moreover, in the calibration test for the nitrile-Perspex contact, while as for the metal-metal calibration test, two calibration cylinders made from nitrile and Perspex were used, it was hard to achieve an even pressure distribution in the nominal contact area. Instead it divided into several regions possessing different pressure levels, as shown in Figure 8, because of the low Young's Modulus of nitrile. Therefore, rather than directly obtaining a uniform ***K*** value in metal-metal contact calibration, multiple ***K*** samples from low-pressure level regions to high-pressure regions were selected for each load.

Without losing generality, mean values were taken from 100 elements randomly selected within the contact region of the stiffness matrix and the process was repeated for 10 cycles to ensure both high stress regions and low stress regions were covered. Consequently, 10 calibration stiffness values can be obtained from each stiffness map under specific load. Since the regression process is not applicable to multivalued functions, the ***K-p*** scatter plot was transposed to give a ***p-K*** scatter plot as shown in Figure 9.

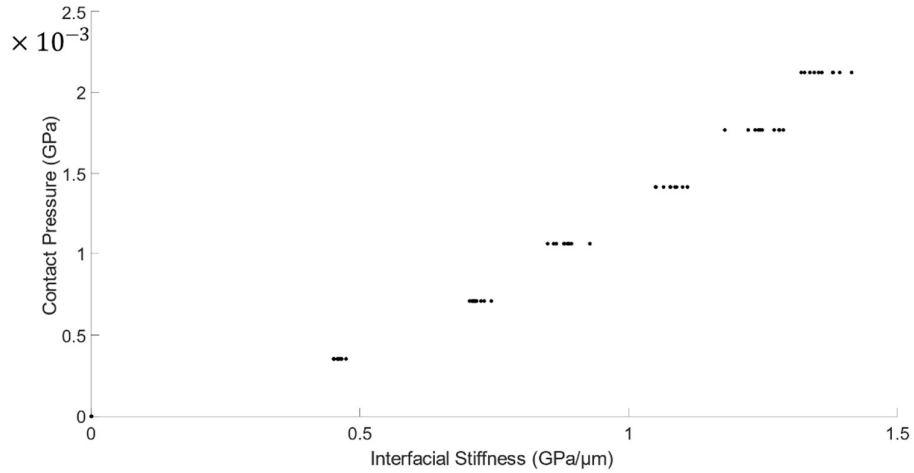

Figure 9. Scatter plot of ***p-K*** relationship from calibration measurements.

It can be clearly seen from Figure 9 that the interfacial stiffness exhibits a non-linear trend as it rises with an increasing load. Besides, the separation of each 10-sample dataset is also gradually growing subject to the increasing load. Under higher load, the variance of the K values becomes higher, exhibiting a heterogenous variance pattern. In this case, a straight line can no longer be used to fit the data using the conventional least mean square approach. To rapidly find a regression model for the ***K-p*** relationship in this study, a variational heteroscedastic Gaussian Process (VHGP) regression algorithm was used [43].

Figure 10 presents the ***p-K*** VHGP regression model with an array of interfacial stiffness measurements from the static ball-on-plate test. The red line is the mean value of output distribution of $\boldsymbol{p}_*$ and the two black lines mark the boundary of 95% confidence interval. In this study, to obtain a bijection ***p-K*** relationship, the mean value is directly used to map each ***K*** value from Figure 8(b) to ***p***.

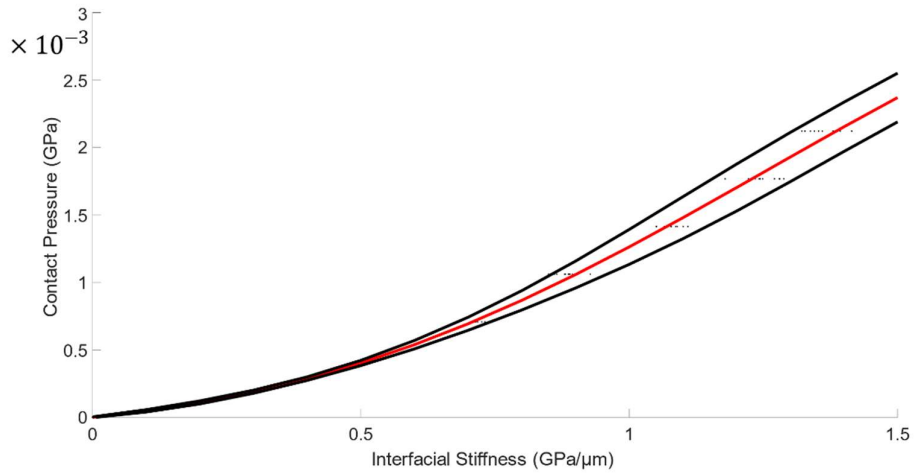

Figure 10. The ***p-K*** VHGP regression model with 95% interval of confidence.

3.2.2 Static results

In the static test, a series of loads from 10N to 50N at 10N steps were applied. Figure 11 displays the distribution maps of reflection coefficient and interfacial stiffness under varying loads.

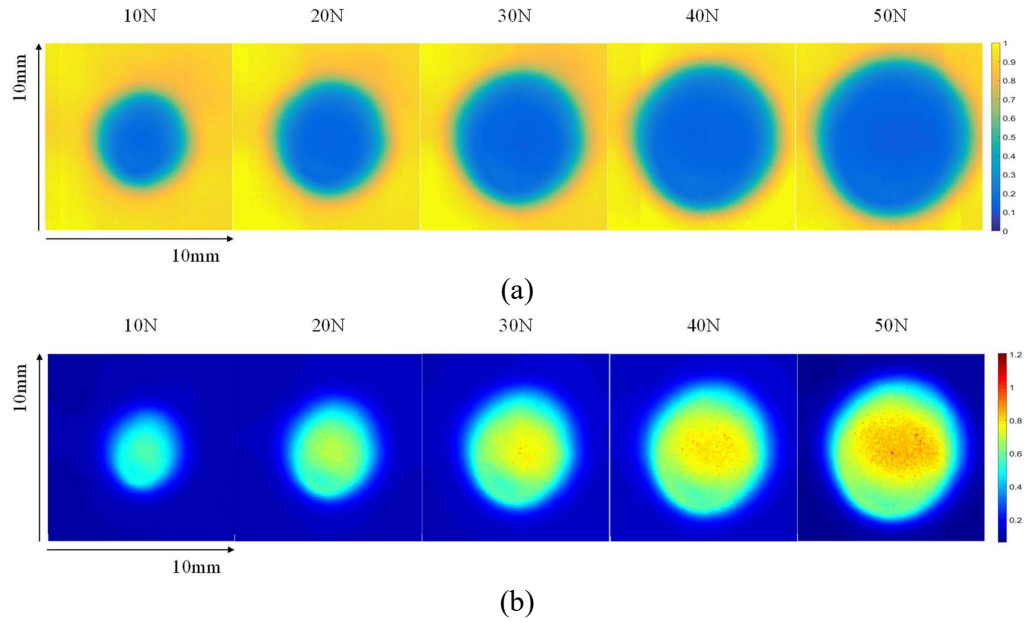

Figure 11. Distribution maps of (a) reflection coefficient; (b) interfacial stiffness in static test.

The contact pressure maps of the static nitrile ball-Perspex plate test can be plotted by feeding each row/column of interfacial stiffness maps into the ***p-K*** model obtained from the calibration test, as shown in Figure 12.

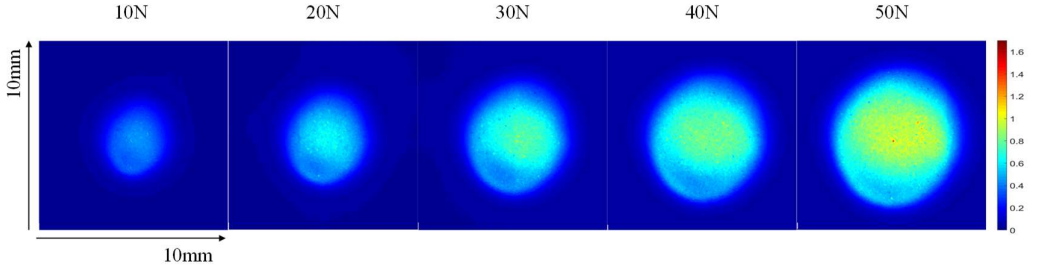

Figure 12. Distribution maps of contact pressure in static test (MPa).

The reflection coefficient maps can help in visualizing the size and shape of contact patch, which is expanding correspondingly under increasing loads. It should be admitted that due to slight movement of the holding plate in the test, the applied load was not fully normal to the contact plane, hence the contact patches are not perfectly circular. The pressure and contact size results will be further compared with dynamic results presented in the next sub-section, as well as those obtained from other methods for validation.

3.2.3 Dynamic results

Figure 13 presents the 2D maps of reflection coefficient, interfacial stiffness and contact pressure under three speeds and five loads. To better view the results and the contact patches, the distribution matrices are interpolated, and contact pressure distribution maps are zoomed in.

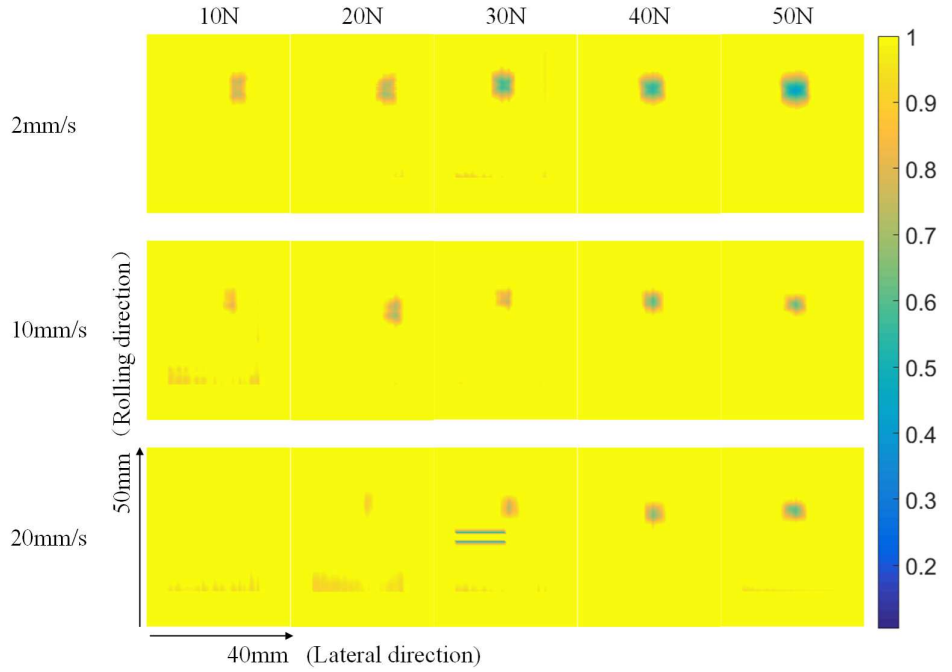

(a)

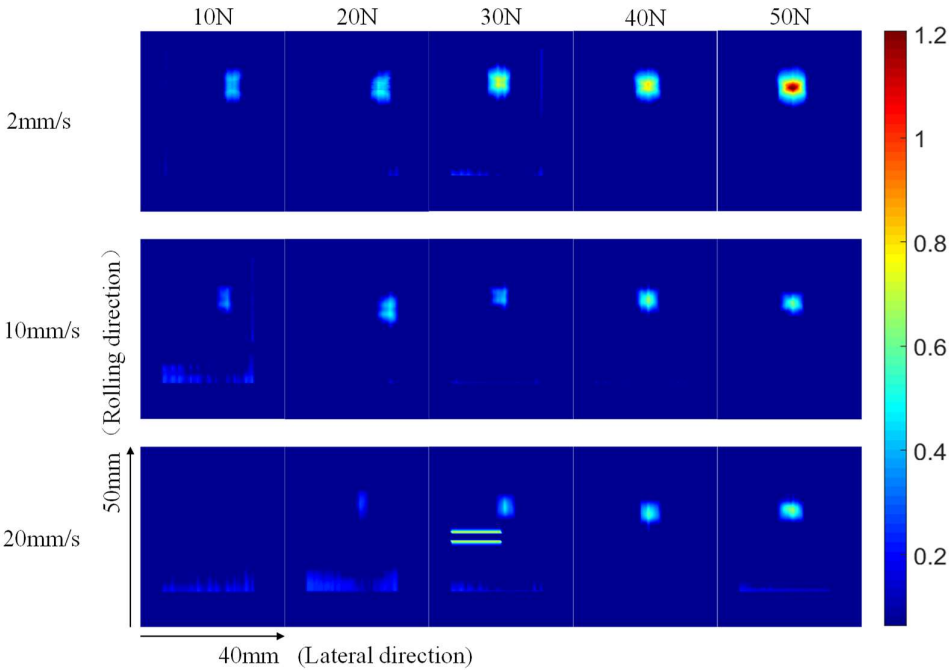

(b)

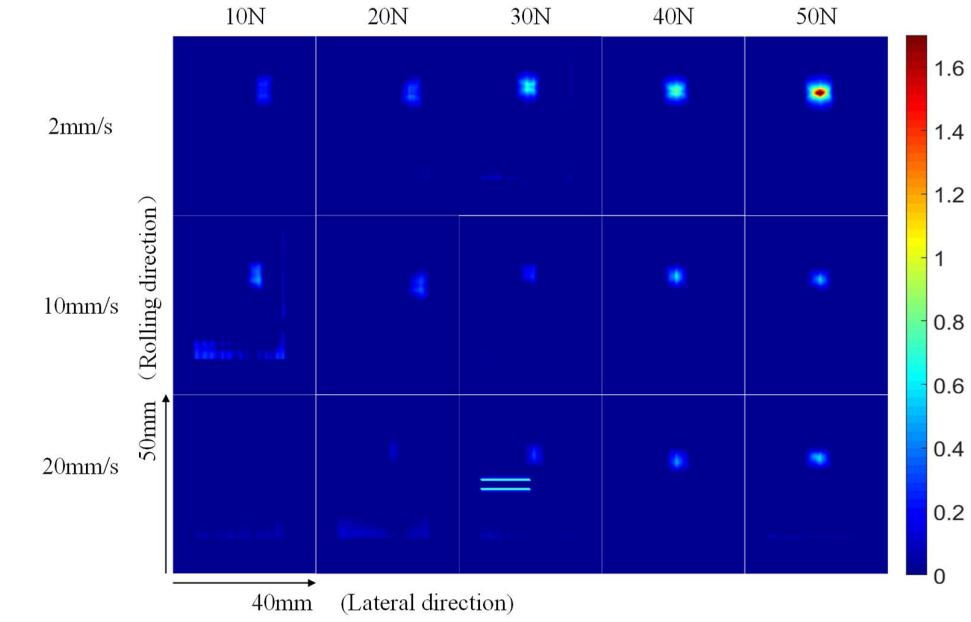

(c)

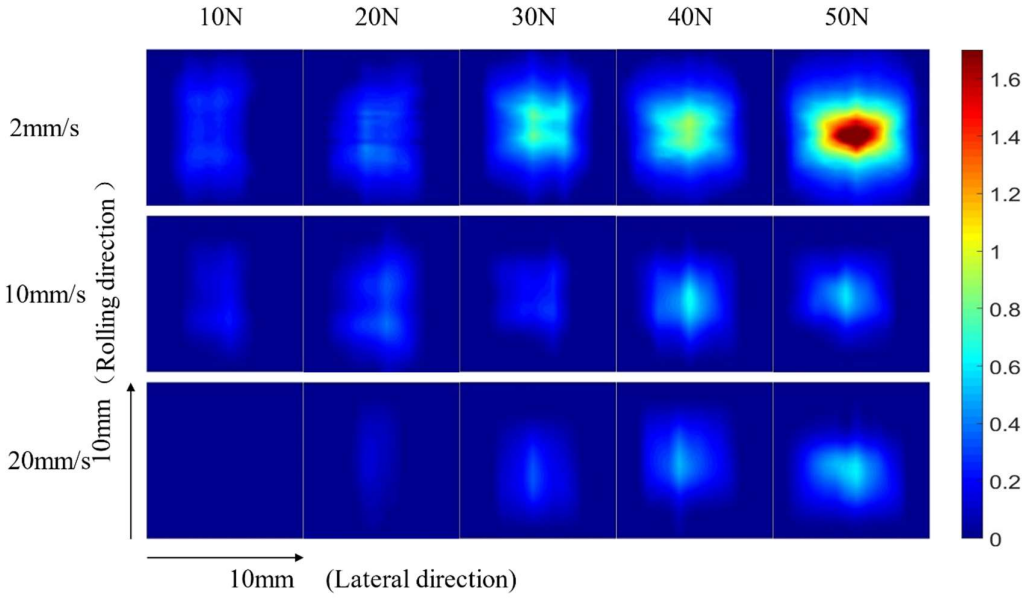

(d)

Figure 13. Distribution maps of: (a) reflection coefficient; (b) interfacial stiffness (GPa/μm); (c) contact pressure in dynamic test (MPa); (d) zoomed in contact pressure in dynamic test (MPa).

Different from static tests, the resolution of dynamic scans along lateral direction is determined by the number of sensing elements (64) in the ultrasonic array, and the resolution along longitudinal direction is determined by the pulsing speed v_p of ultrasonic pulser, switching speed of the multiplexer and the rolling speed v_r of the nitrile ball. The higher the v_p/v_r ratio is, the more effective the information is that can be acquired. Because the pulsing speed was fixed in all dynamic tests, measurements

taken at a speed of 2mm/s provides the most detailed contact information. As with those taken under 10mm/s and 20mm/s, although the contact patch and distribution of contact pressure are indicated, neither are as clear or accurate. Therefore, the measurements under 2mm/s were primarily used for comparison in the next sub-section. However, it should also be noted that the switching speed of the multiplexer limited the speed measurements could be taken at, so even the fastest rolling speed in the dynamic test is far lower than real applications. It is expected, however, that the applied speed can be enhanced upon upgrading of the multiplexer.

3.3 Validation and discussion

The ultrasonic measurements can be quickly validated through Hertz theory. Because the nitrile-Perspex contact is associated with large deformation and nonlinear behaviour which goes beyond the assumption of Hertz, finite element (FE) simulation was also conducted as a second validation approach. Theoretically speaking, the static contact should be identical with the pure rolling contact (zero creepage), which makes ultrasonic measurements from the static test and dynamic test comparable.

3.3.1 Hertz prediction for sphere-plate contact

For this study, the Perspex plate was regarded as a sphere with infinite radius, while the radius of the nitrile ball is 13mm. Referring to Table 1, the Hertz predictions can be quickly calculated.

3.3.2 FE simulation

As for contacts with non-linear behaviours, comparison with results from various approaches besides Hertz predictions are preferred. A ball-on-plate contact model was simulated in ANSYS referring to elastic properties in Table 1. The structural mesh element was SOLID186 with mesh size set to be 1mm, and the contact mesh element was CONTAC174 for contact surface and CONCAC170 for target surface with mesh size set to be 0.1mm, as shown in Figure 14. The solver algorithm was pure penalty and large deformation option was switched on. Nodes within the contact region and the contact neighbourhood were selected with corresponding simulation results extracted in matrix for easy data processing and interpretation. Figure 15 displays the simulated pressure distribution under normal load from 10N to 50N.

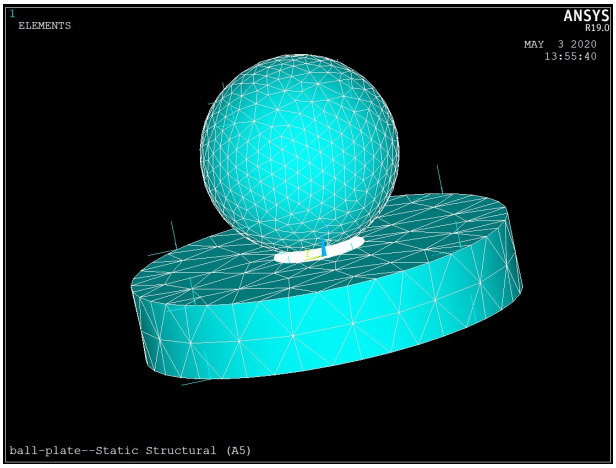

Figure 14. Finite element model of nitrile ball-Perspex plate contact.

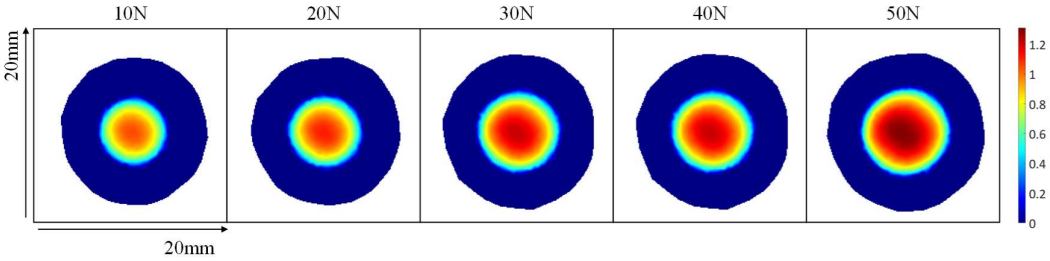

Figure 15. FE simulation results of nitrile ball-perspex plate contact pressure (MPa).

3.3.3 Picture validation

The transparency of Perspex offers a straightforward way to validate the contact size. Pictures were taken from a mounted camera under increasing load, as shown in Figure 16.

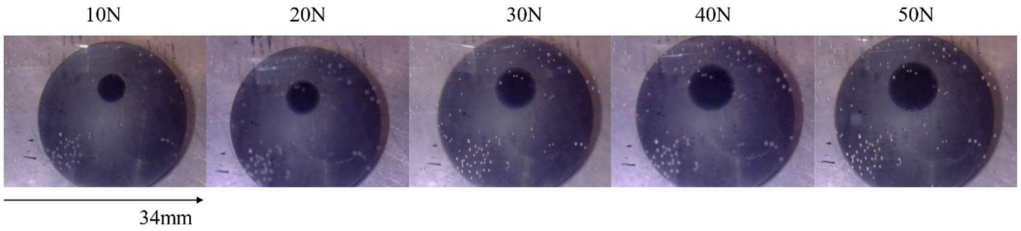

Figure 16. Pictures of nitrile-Perspex contact patches.

3.3.4 Result comparison and discussion

Contact size (diameter) and peak contact pressure from the static test, dynamic test, Hertz prediction and FE simulation were compared, as shown in Figure 17. For contact size comparison, boundary of contact regions in the ultrasonic measurements were identified based on the specified threshold of reflection coefficient referring to authors' previous work [26,27]. For contact pressure comparison, since pressure distribution of ball-on-plate contact theoretically follows a spherical distribution, the peak contact pressure value can be a representative indicator. It should be noted, however, that according to Figure 13 and 15, ultrasonic measurements tend to have larger variations

and are likely capture outlier peak pressure values. To achieve a more general view, averaged peak pressure calculated from a 10% contact radius neighbourhood centred at the peak pressure spot was also included for comparison. Peak pressures were plotted as solid lines and averaged peak pressures were plotted as dashed lines.

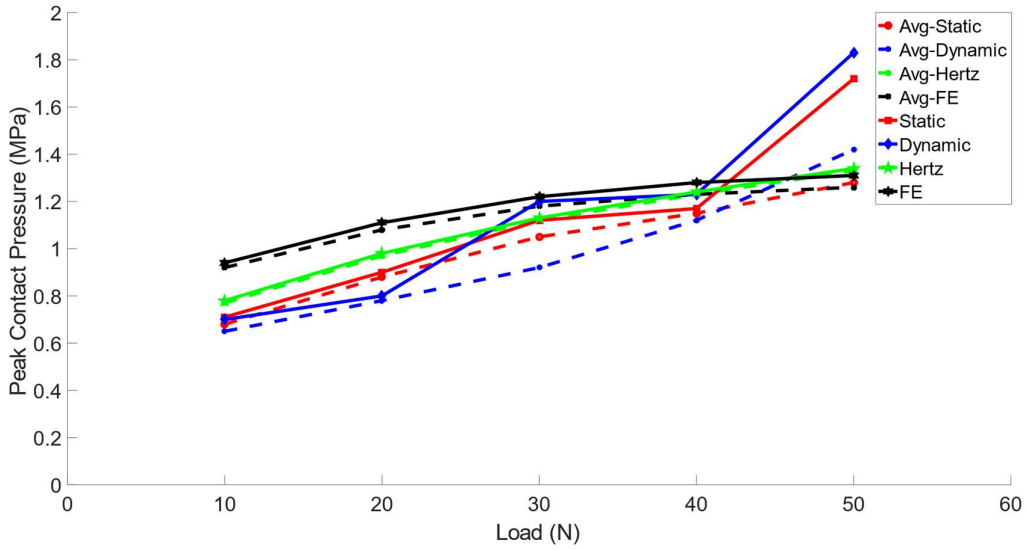

(a)

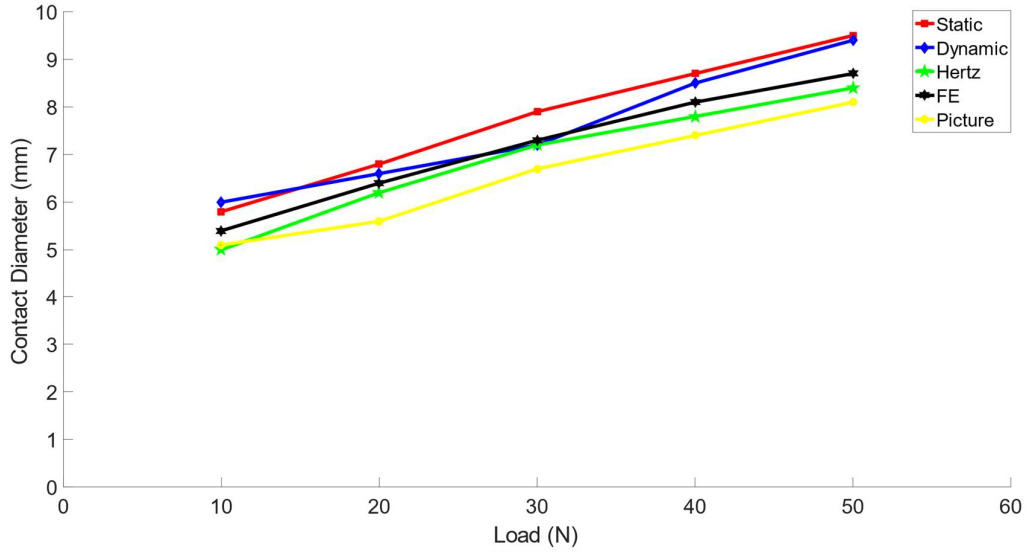

(b)

Figure 17. (a) Contact diameter; (b) peak pressure comparison between ultrasonic measurements and other validation methods.

From Figure 17(a) it can been observed that results from static and dynamic tests match with each other well as expected for pure rolling contacts. Both results also agree well with Hertz predictions. Subject to stochastic influencing factors (subtle test condition difference, signal fluctuations, etc.) in each run, peak pressure values from the ultrasonic measurements exhibit a larger and more unsteady growth rate than Hertz

predictions and FE simulations under increasing load. Because the effective number of measurements of dynamic scanning is smaller than that of static scanning, peak pressure in dynamic test is varying in a slightly larger range than that in the static test. Due to the asperity contact in real cases, the stress tends to concentrate more within the contact zone under higher loads, hence the experimental measurements appear to be bigger than other results. When it comes to averaged peak pressure, the pressure curves of both static and dynamic ultrasonic measurements show a further satisfactory agreement with validations in terms of growth rate and magnitude, but slightly smaller, indicating that pressure drops faster than Hertz prediction and FE simulation in the neighbourhood of the peak pressure spot.

As with contact size, good agreement can also be seen in Figure 17(b) where the growth trend is almost the same and the diameter is growing within the 5-10mm range under increasing load among all evaluation methods. Contact patches measured in static and dynamic conditions are basically 10%-20% larger in diameter than those from validation methods. This is mainly due to the edge effect of ultrasonic reflectometry which refers to the mechanism that when a sensing element scans over the boundary of contact area, it takes convolutional average of the entire scanning area/focusing spot as a single measurement, leading to a larger contact patch than both theoretical prediction and actual vision validation.

4. Real-time monitoring of steel ball-on-grooved plate rolling contact

To test the applicability of the technique in real-time monitoring of dynamic contacts of specific machine elements such as rolling element bearings, the contact between a steel ball and a steel plate with a curved groove, which mimics the topological structure of ball bearing, was measured with the ultrasonic array. Limited by the size and shape of the array, and also for better demonstration purpose, a bearing was not used in this study. To simulate the real scenarios, the radius of the steel ball in the test was 11mm, and the radius of the curved groove was 10.5mm. According to Hertz prediction, if the radius of the groove is smaller than ball radius, the contact patch would be two ovals with each located at one edge of the groove. This is also verified through a quick static test on the contact pair, as shown in Figure 18.

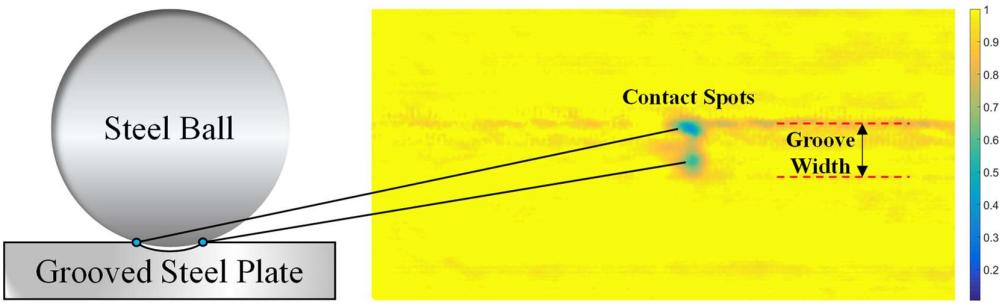

Figure 18. Steel ball-on-grooved steel plate contact and static scanning (1kN load)

4.1 Test set-up

A rotary test rig was designed and developed to conduct the investigation, as shown in Figure 19. A steel plate was placed on three steel balls (11mm radius) which were kept in position with ball holders. The steel balls were positioned equal-distantly with a 120-degree separation from each other, and the ball holders contain bearing mechanism to allow the steel balls to rotate freely. A 7mm wide, 0.6mm deep (i.e., the groove radius is 10.5mm) grooved ring had been machined on the bottom side of the plate. Radial positions of the ball holders were adjusted so that the steel balls were in the neutral axis of the groove for symmetrical contact patches. The plate was driven by a motor to enable rotational movement, and the ultrasonic array was clamped on top of the rotating plate with the cable bind to the axle. The distance from the neutral axis of the groove to the rotating axle is 60mm. When the array moved into the contact region, contact was detected by part of the sensing elements in the ultrasonic array.

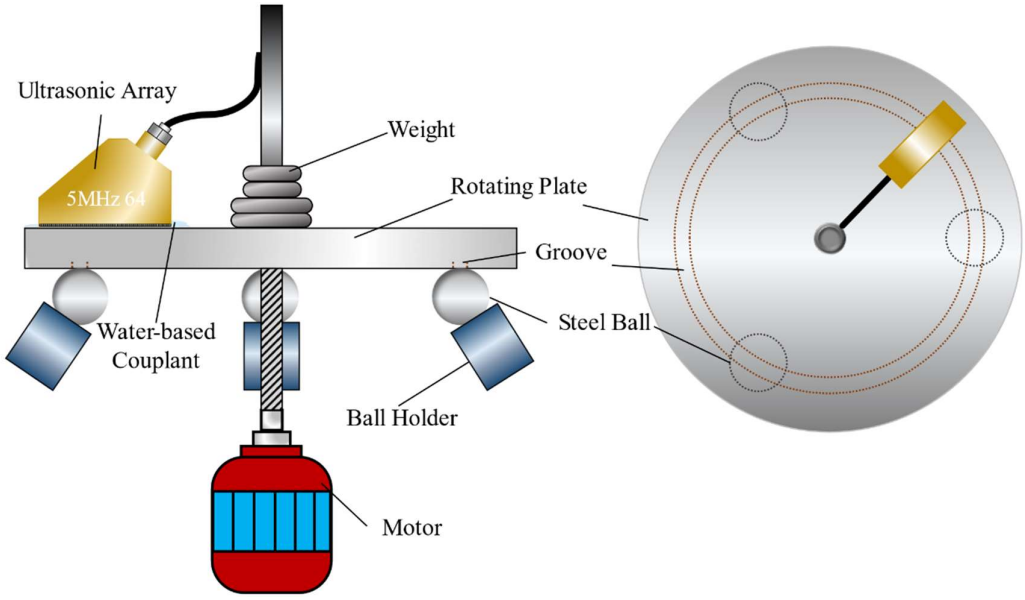

Figure 19. Steel ball-on-grooved steel plate rolling contact test rig

It should be noted that since the contact patch between the steel ball and the grooved plate is much smaller than that of the nitrile ball-perspex plate contact, it is located within the scanning range of at most 4 to 5 sensing elements of the ultrasonic array. Besides, it is not feasible to integrate a loading system for the test rig, and the applied normal load is relatively limited (so is the case for realistic in-service bearing). Therefore, this test serves as a pilot study to convey the conceptual idea with a fixed weight load applied.

4.2 Scanning result

Measurements were taken for a full cycle of rotation (period: 80s), so that contacts between the plate and all three balls were detected. 100kg weight (maximum affordable weight of the test rig) was applied. A reference test was carried out without any load to partially eliminate the bias induced by the curved profile. Figure 20 shows the scanning map of reflected voltage and reflection coefficient with 32 “contact-close” sensors in the ultrasonic array used for plotting.

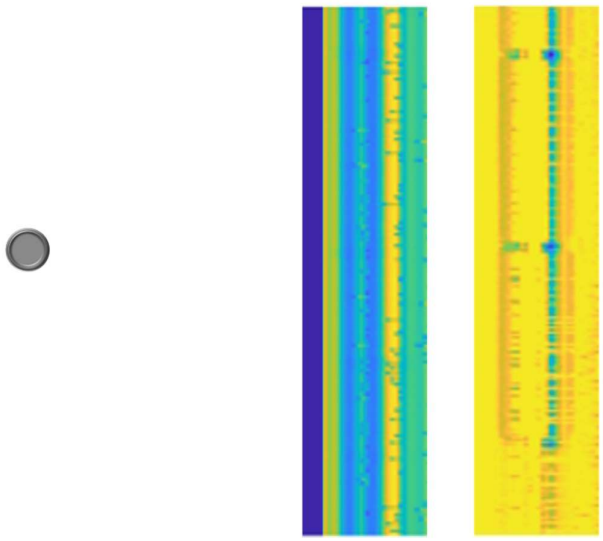

Figure 20. Reflected voltage and reflection coefficient map of steel ball-on-grooved plate rolling contact test.

It can be seen from the reflection coefficient map that contacts between the rotating plate and all three balls were detected, and the two contact spots on two edges of the groove were clearly captured. This is in alignment with predictions as well as the static scanning results. The equal distance between the detected contacts corresponds to the centrosymmetric placement of the balls. As stated above, the contact patch of a steel-steel contact pair under a 1kN load is extremely small (less than 0.3mm), and the resolution of dynamic scanning is relatively limited. The visualised contact patch is more related to the edge effect of ultrasonic reflectometry, and pressure determination at this stage is likely to be inaccurate. However, the result can approximately quantify the contact state. A side view of the reflection coefficient map is shown in Figure 21. From Figure 21 it can be inferred that despite of the adjustment of ball position in test set-up for a symmetrical contact, uneven contact took place during the rotating test. This can be a useful in real-time monitoring the operating condition of rotary bearings in practical applications. Besides, from the side view of the reflected voltage map it can also be observed how the curved surface profile may influence the measurements, confirming the necessity of choosing reference measurements appropriately to eliminate the profile influence.

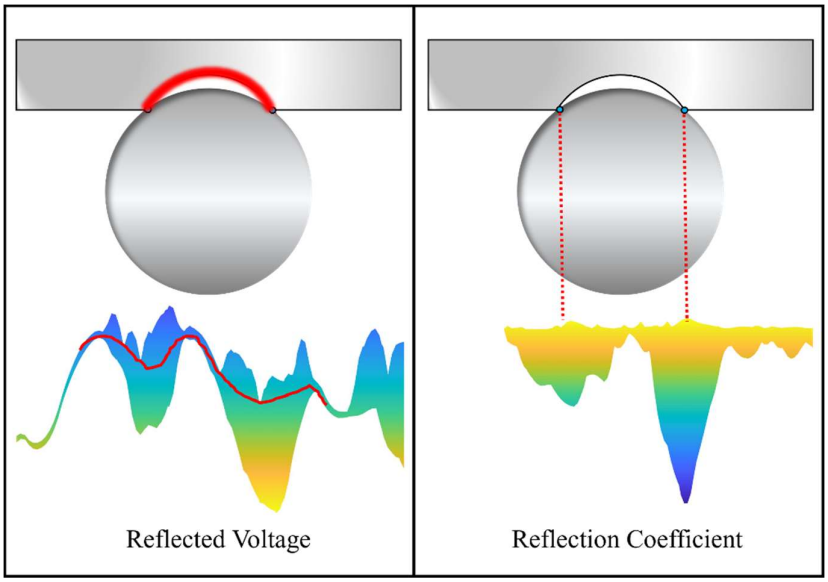

Figure 21. Side view of reflected voltage and reflection coefficient of steel ball-on-grooved plate rolling contact test.

5. Conclusions

To summarize, this paper introduces the experimental investigation of ball-on-plate contacts in a real-time manner by using an ultrasonic reflectometry measuring technique. To realize contact characterisation under different scenarios (static and dynamic, metal and non-metal), ultrasonic focusing transducers and a 64-element ultrasonic array were used, and a federation of mechanisms were designed and developed.

Static and dynamic contacts of a nitrile ball against a Perspex plate were characterised. While the authors have previously conducted a series of research studies on contact characterisation using ultrasonic reflectometry, this study for the first time systematically investigates contacts between non-metal materials with large deformation. Although the measuring process in a metal-metal contact test and a non-metal contact test is the same, the ***K-p*** relationship needs to be established in a different way. In face of the calibration test challenges brought about by non-linear contact behaviours and large deformation with significant stochasticity, Gaussian Process regression was used to derive the ***K-p*** relationship in variational distributions rather than a fixed line. This can also be a feasible way for characterising other non-metal and non-linear contacts. Despite of some fluctuations, the ultrasonic results generally exhibited a satisfactory agreement with different validation methods in terms of both contact size and pressure level, and contacts characterised by ultrasounds can reflect information more relevant to realistic contact conditions than theoretical predictions and FE simulations. In particular, the dynamic measurements can provide sufficiently detailed and accurate contact information with acceptable resolution loss, demonstrating the technique has great potential in providing real-time and reliable information of dynamic contacts in a truly non-invasive manner, while most of the

existing experimental measuring techniques are either destructive or intrusive and can only provide very limited contact information.

A steel ball-on-grooved steel plate mechanism was designed and built up as a pilot study on the applicability of the ultrasonic reflectometry technique in monitoring contacts in bearing-like structures. Although the monitored steel-steel contact patch is small, all contacts were detected and visualised, and contact states can still be vaguely indicated with limited number of effective measurements. Moreover, this test presents new thinking on sensor/array implementation on moving/rotary structures such as rolling wheels, as a potential progress on existing dynamic wheel-rail contact monitoring technique developed by the authors [28, 29, 30].

Despite the effectiveness of the proposed measuring technique in characterising static and dynamic contacts demonstrated in this study, it should be noted that there are still several limitations yet to be improved before application on operating rolling element bearings: 1. Limited by the available hardware (ultrasound pulsing speed, physical size of ultrasonic sensing elements), currently only dynamic contacts at relatively low speeds can be characterized with adequate details; 2. The ultrasonic array used in this study is not suitable for monitoring contacts of small bearings; 3. In real applications, the host structure can be complex with multiple thin layers which leads to multiple reflections in the time domain, making it tricky to extract the reflection of interest. Hardware upgrading work is in progress including increasing pulsing speed which is expected to detect rolling contacts at much higher speeds [27], and fabrication of smaller and 2D PCB-based ultrasonic array applicable for smaller more delicate contact environment.

References

[1] L. Sosnovskii (2003). "Mechanical State Analysis of Load-Bearing Systems. Part 1. The Ultimate State", *Strength of Materials*, 35(5): 458-467.

[2] Y. Okamoto (2000). "A study for wear and fatigue on engine bearings by using EHL analysis", *JSAE Review*, 21(2):189-196.

[3] F. Braghin, R. Lewis, R. Dwyer-Joyce and S. Bruni (2006). "A mathematical model to predict railway wheel profile evolution due to wear", *Wear*, 261(11-12):1253-1264.

[4] T. Telliskivi and U. Olofsson (2001). "Contact mechanics analysis of measured wheel-rail profiles using the finite element method", *Proceedings of the Institution of Mechanical Engineers, Part F: Journal of Rail and Rapid Transit*, 215(2):65-72.

[5] P. Põdra, S. Andersson (1999). "Finite element analysis wear simulation of a conical spinning contact considering surface topography", *Wear*, 224(1): 13-21,

[6] A. Chasalevris, F. Dohnal, I. Chatzisavvas (2014). "Experimental detection of additional harmonics due to wear in journal bearings using excitation from a magnetic bearing", *Tribology International*, 71:158-167.

[7] T. J. Harvey, R. J. K. Wood, H. E. G. Powrie (2007). "Electrostatic wear monitoring of rolling element bearings", *Wear*, 263(7–12):1492-1501.

[8] Y. Jin, M. Ishida and A. Namura (2011). "Experimental simulation and prediction of wear of wheel flange and rail gauge corner", *Wear*, 271(1-2):259-267.

[9] H. Brunskill, P. Harper, R. Lewis (2015). "The real-time measurement of wear using ultrasonic reflectometry", *Wear*, 332–333:1129-1133.

[10] H. Hertz (1882). "Ueber die Berührung fester elastischer Körper.", *Journal für die reine und angewandte Mathematik (Crelles Journal)*, 1882(92):156-171.

[11] S. Hunter (1961). "The Rolling Contact of a Rigid Cylinder with a Viscoelastic Half Space", *Journal of Applied Mechanics*, 28(4):611-617.

[12] E. Kral, K. Komvopoulos and D. Bogy (1993). "Elastic-Plastic Finite Element Analysis of Repeated Indentation of a Half-Space by a Rigid Sphere", *Journal of Applied Mechanics*, 60(4):829-841.

[13] A. Majumdar and B. Bhushan (1991). "Fractal Model of Elastic-Plastic Contact Between Rough Surfaces", *Journal of Tribology*, 113(1):1-11.

[14] B. Bhushan and A. Majumdar (1992). "Elastic-plastic contact model for bifractal surfaces", *Wear*, 153(1):53-64.

[15] A. Goedecke, R. L. Jackson, R. Mock (2013). "A fractal expansion of a three dimensional elastic–plastic multi-scale rough surface contact model", *Tribology International*, 59:230-239.

[16] W. Poole (1987). "The measurement of contact area between opaque objects under static and dynamic rolling conditions", *Proceedings of Contact Mechanics and Wear of the Wheel/rail System*, University of Rhode Island, Waterlooville Press, pp. 59-72.

[17] F. P. Bowden, D. Tabor (1950). *The Friction and Lubrication of Solids*, Clarenden Press, Oxford, 432 pages.

[18] H. Fesseler, E. Ollerton (1957). “Contact Stresses in Toroids Under Radial Loads”, *British Journal of Applied Physics*, 8(10):387-393.
[19] K. N. Bachus, A. L. DeMarco, K. T. Judd, D. S. Horwitz, D. S. Brodke (2006). “Measuring contact area, force, and pressure for bioengineering applications: Using Fuji Film and TekScan systems”, *Medical Engineering & Physics*, 28(5): 483-488.
[20] J. Z. Wu, W. Herzog, M. Epstein (1998). "Effects of Inserting a Pressensor Film into Articular Joints on the Actual Contact Mechanics." *ASME. Journal of Biomechanical Engineering*, 120(5): 655–659.
[21] M. Jalalpour, J. J. Kim, M. M. Reda Taha (2013). “Monitoring of L-Shape Bolted Joint Tightness Using Thermal Contact Resistance”, *Experimental Mechanics*, 53:1531–1543.
[22] S. Descartes, C. Desrayaud, Y. Berthier (2008). “Experimental identification and characterization of the effects of contaminants in the wheel—rail contact”, *Proceedings of the Institution of Mechanical Engineers, Part F: Journal of Rail and Rapid Transit*, 222(2):207–216.
[23] M. B. Marshall, R. Lewis, R. S. Dwyer-Joyce, U. Olofsson, S. Björklund (2006). "Experimental Characterization of Wheel-Rail Contact Patch Evolution", *ASME. Journal of Tribology*, 128(3):493-504.
[24] M. B. Marshall1, R. Lewis, B. W. Drinkwater, R. S. Dwyer-Joyce (2004). “An ultrasonic approach for contact stress mapping in machine joints and concentrated contacts”, *Journal of Strain Analysis for Engineering Design*, 39(4): 339–350.
[25] U. Fernando, P. Nott, G. Graham, A. Roberts, T. Sheldrake, H. P. Brunskill, L. Zhou, R. Lewis (2012). “Experimental Evaluation of the Metal-to-Metal Seal Design for High-Pressure Flexible Pipes”, in *Proceedings of the Offshore Technology Conference*, 30th April-3rd May 2012, Houston, Texas, USA.
[26] R. S. Dwyer-Joyce, B. W. Drinkwater, C. J. Donohoe (2003). “The measurement of lubricant–film thickness using ultrasound”, *Proceedings of the Royal Society A: Mathematical, Physical and Engineering Sciences*, 459:957–976.
[27] R. S. Dwyer-Joyce, T. Reddyoff, B. W. Drinkwater (2004). “Operating Limits for Acoustic Measurement of Rolling Bearing Oil Film Thickness”, *Tribology Transactions*, 47(3):366-375.
[28] L. Zhou, H. P. Brunskill, R. Lewis, M. Pletz, W. Daves, S. Scheriau (2019). “Real time Measurement of Dynamic Wheel-Rail Contacts Using Ultrasonic Reflectometry”, *ASME. Journal of Tribology*, 141(6):061401, 9 pages.
[29] L. Zhou, H. P. Brunskill, R. Lewis (2019). “Real-time non-invasive measurement and monitoring of wheel–rail contact using ultrasonic reflectometry”, *Structural Health Monitoring*, 18(56):1953-1965.
[30] H. Brunskill, A. Hunter, R. S. Dwyer-Joyce, R. Lewis (2020). “An evaluation of ultrasonic arrays for the static and dynamic measurement of wheel–rail contact pressure and area”, *Proceedings of the Institution of Mechanical Engineers, Part J: Journal of Engineering Tribology*.
[31] M. Hong, Q. Wang, Z. Su, L. Cheng (2014). “In situ health monitoring for bogie systems of CRH380 train on Beijing–Shanghai high-speed railway”, *Mechanical*

System and Signal Processing, 45:378-395.

[32] S. Coccia, I. Bartoli, A. Marzani, F. L. di Scalea, S. Salamone, M. Fateh (2011). "Numerical and experimental study of guided waves for detection of defects in the rail head", *NDT & E International*, 44(1):93-100.

[33] Q. Huan, M. Chen, Z. Su, F. Li (2019). "A high-resolution structural health monitoring system based on SH wave piezoelectric transducers phased array", *Ultrasonics*, 97:29-37.

[34] J. F. Synnevag, A. Austeng and S. Holm (2007). "Adaptive Beamforming Applied to Medical Ultrasound Imaging", in *IEEE Transactions on Ultrasonics, Ferroelectrics, and Frequency Control*, 54(8):1606-1613.

[35] L. Satyanarayan, C. Sridhar, C.V. Krishnamurthy, K. Balasubramaniam (2007). "Simulation of ultrasonic phased array technique for imaging and sizing of defects using longitudinal waves", *International Journal of Pressure Vessels and Piping,* 4(12):716-729.

[36] K. Kendall, D. Tabor (1971). "An Ultrasonic Study of the Area of Contact between Stationary and Sliding Surfaces", *Proceedings of the Royal Society, Series A*, 323:321-340.

[37] B. W. Drinkwater, R. S. Dwyer-Joyce, P. Cawley (1996). "A Study of the Interaction between Ultrasound and a Partially Contacting Solid-Solid Interface", *Proceedings of the Royal Society Series A*, 452:2613-2628.

[38] Designerdata. https://designerdata.nl/materials/plastics/rubbers/nitrile-butadiene-rubber.

[39] Designerdata. https://designerdata.nl/materials/plastics/thermo-plastics/poly(methyl-methacrylate)

[40] J. Krautkrämer, H. Krautkrämer (1990). *Ultrasonic Testing of Materials* (fourth edition), Springer, Berlin, 677 pages.

[41] M.B. Marshall (2005) "An Ultrasonic Investigation of Real Engineering Contacts", PhD Thesis, The University of Sheffield.

[42] T. H. Gan, D. A. Hutchins, D. R. Billson, D. W. Schindel (2001). "The use of broadband acoustic transducers and pulse-compression techniques for air-coupled ultrasonic imaging", *Ultrasonics*, 39(3):181-194.

[43] M. Lázaro-Gredilla, M. K. Titsias (2011). "Variational Heteroscedastic Gaussian Process Regression", *Proceedings of the 28th International Conference on Machine Learning*, ICML 2011, Bellevue, WA, USA, 841-848.